Temperature and bias dependences of defect mode in a photonic crystal containing a photonic-quantum-well defect

YANG-HUA CHANG, YING-YAN JHU[a], CHIEN-JANG WU[b*]
Department of Electronic Engineering, National Yunlin University of Science and Technology, Yunlin 640, Taiwan
[a]*Graduate School of Optoelectronics, National Yunlin University of Science and Technology, Yunlin 640, Taiwan*
[b]*Institute of Electro-Optical Science and Technology, National Taiwan Normal University, Taipei 116, Taiwan*

The temperature- and bias-dependent properties of the defect mode in a one-dimensional photonic crystal (1D PC) containing a photonic-quantum-well (PQW) defect are theoretically investigated. The temperature dependence is studied by simultaneously incorporating thermal expansion and thermal-optical effects in the constituent layers. As the thickness and index of refraction of each layer are modulated by temperature, a tunable filter working in the visible region is proposed. The shift of transmittance peak per 100 °C is around 2 nm, depending on the value of *m*, which is the stack number of the PQW and ranges between 1 and 3 in our study. It is found that the third transmittance peak in the case of *m* = 3 is most sensitive to temperature (2.43 nm per 100 °C), whereas the second transmittance peak of *m* = 3 is the sharpest. The bias dependence is studied by considering the electro-optic effect of the defected layer. The shifts of transmittance peaks are found to be in the range of 0.129 ~ 0.188 nm per 1 kV of applied voltage. Additionally, the second transmittance peak of *m* = 3 is most sensitive to voltage, and it is also the sharpest peak.

(Received January 2, 2012; accepted April 11, 2012)

Keywords: Photonic crystal, Photonic quantum-well, Thermal effect, Electro-optic effect

1. Introduction

The concept of photonic crystals (PCs) was first proposed by Yablonovitch and John in 1987 [1,2], who found that using periodic arrangement of dielectric materials enables us to control the propagation of electromagnetic waves. The most significant feature of a PC is the existence of photonic band gap (PBG), a frequency range in which the electromagnetic waves cannot propagate. The PBG in a PC is analogous to the electronic band gap in a solid because of the similarity between the structural periodicity of a PC and the periodic potential energy in a solid. If the periodicity of the PC is interrupted, such as the thickness of a layer being changed [3], or another medium being added into the structure [4], some defective modes could be generated within the PBGs. In a simple one-dimensional PC of $(AB)^n$, the defect mode can be obtained in a defective structure like $(AB)^nD(AB)^n$, where D is known as a defected layer. The defect mode is a strongly localized defect state which, in general, can be seen in the transmission spectrum with a sharp narrow resonant peak. With the presence of resonant peak in transmittance, the structure is often used as a narrowband transmission filter [5].

The defected layer added to a PC of $(AB)^n$ can be replaced by another PC of $(CD)^m$ such that the structure is $(AB)^n(CD)^m(AB)^n$, where *n* and *m* are the stack numbers of the (AB) and (CD) bilayers, respectively. In this case, the defect, $(CD)^m$, is known as the photonic quantum well (PQW) [6-8]. If one of the pass band of $(CD)^m$ can be designed to completely overlap with one of the PBGs of the host PC of $(AB)^n$, the structure $(AB)^n(CD)^m(AB)^n$ (with $m < n$) can then exhibit multiple filtering property because of the photonic confinement, leading to a realization of a multichannel filter [6]. In addition, the number of channels, i.e., the number of peaks in the transmission spectrum, is just equal to *m*, the stack number of PQW. With this idea, some related multichannel narrowband transmission filters have been theoretically studied thus far [6-10]. Some experimental works using the PQW have also been reported [11-12]. The multichannel filters are advantageous to constructing the dense wavelength division multiplexing (DWDM) filter which is of particular use in optical communications.

Although there have been many reports on filters based on PQW [6-10], few studies focus on tunable multichannel transmission filters. Tunable filters have been attractive photonic applications. The tunable feature can be achieved by various external agents, such as the change in temperature [13-15], the applied external bias voltage [16], the change in incident angle [17], and the use of mechanical modulation in metallic photonic crystal [18-19].

In this work, we design tunable multichannel transmission filters working in the visible region by temperature variation and external applied bias voltage.

We first consider a 1D PC containing PQW defect that is designed by using the temperature modulation in thickness (thermal expansion effect) and index of refraction (thermal-optical effect) on each layer. By simultaneously incorporating these effects, we design a structure of $(HL)^n(DL)^m(HL)^n$, where H and L stand for the media with high and low indices of refraction, respectively. Si is used for layer H, and SiO_2 is used for layer L. $(DL)^m$ stands for the PQW defect. $Bi_4Ge_3O_{12}$ is chosen for D layers. Next, a different material, $LiNbO_3$, is used for D layers to incorporate the electric-field modulation of index of refraction (electro-optic effect), for the design of voltage-modulated multi-channel transmission filter.

2. Basic equations

In this work, a defect-free PC has a structure of $(HL)^{2n}$, while the defective PC to be considered has a structure of $(HL)^n(DL)^m(HL)^n$, in which H and L are respectively the high- and low-index layers, and central part $(DL)^m$ serves as a PQW with D being the third constituent. The structure is shown in Fig. 1.

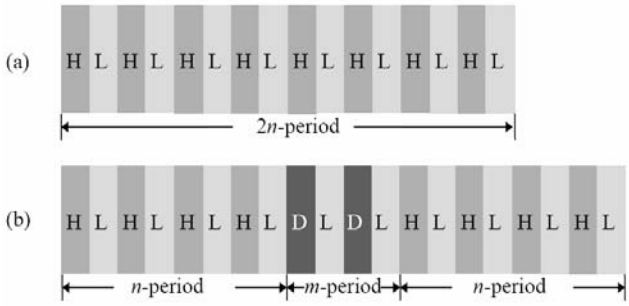

Fig. 1. The structures of (a) $(HL)^{2n}$, and (b) $(HL)^n/(DL)^m/(HL)^n$, taking n = 4 and m = 2 for example. The thickness of H, L, and D layers is 120 nm.

To investigate the properties of the defect modes, we shall use the transmission spectrum which can be calculated by the transfer matrix method (TMM) [20]. According to TMM, each single layer has a transfer matrix given by

$$M_l = D_l P_l D_l^{-1};\ l = \text{H, L, or D}, \tag{1}$$

where the dynamical matrix D_l, in the case of normal incidence, is expressed as

$$D_l = \begin{pmatrix} 1 & 1 \\ n_l & -n_l \end{pmatrix}, \tag{2}$$

and the propagation matrix P_l is defined as

$$P_l = \begin{pmatrix} e^{i\phi_l} & 0 \\ 0 & e^{-i\phi_l} \end{pmatrix}, \tag{3}$$

where the phase ϕ_l is expressed as

$$\phi_l = k_l d_l = \frac{2\pi d_l}{\lambda} n_l. \tag{4}$$

For the entire structure of Air/$(HL)^n(DL)^m(HL)^n$/Air, the total transfer matrix is thus given by

$$M = \begin{pmatrix} M_{11} & M_{12} \\ M_{21} & M_{22} \end{pmatrix} = D_0^{-1} \left(M_H M_L\right)^n \left(M_D M_L\right)^m \left(M_H M_L\right)^n D_0, \tag{5}$$

where D_0 is the dynamical matrix for air. With the matrix elements in Eq. (5), the quantity of interest, transmittance T, can be determined from M_{11}, namely,

$$T = \left| \frac{1}{M_{11}} \right|^2. \tag{6}$$

In what follows, we shall calculate the transmittance in the wavelength domain to demonstrate the properties of the defect modes in the PC containing PQW.

3. Numerical result and discussion

3.1 Temperature dependence of defect modes

Let us start with a defect-free PC $(HL)^8$, as shown in Fig. 1(a), which is designed to have a PBG in the visible region. Here, H is taken to be Si with $n_{Si} = 3.45$, and SiO_2 with $n_{SiO2} = 1.45$ is chosen for layer L. The thickness of both layers is 120 nm. The wavelength-dependent transmittance T of this ideal photonic crystal is shown in Fig. 2. It can be seen from Fig. 2 that there is a PBG in the range 501-641 nm. Our goal is to engineer the PBG to produce defect modes, which can be tuned by temperature. The voltage dependence of the defect modes is presented and discussed next.

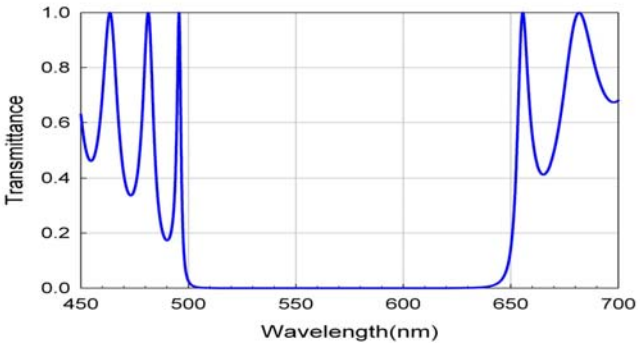

Fig. 2. The wavelength-dependent transmittance for an ideal PC of $(Si/SiO_2)^8$.

In the first part of our work, we add a PQW-defect to the PC $(HL)^8$ such that the structure is $(HL)^4(DL)^m(HL)^4$, as shown in Fig. 1(b). We assume that the whole structure is immersed in the air. Here, D is taken to be $Bi_4Ge_3O_{12}$

(BGO) with index of refraction $n_{BGO} = 2.13$, and m (< 4) is the stack number of PQW. The thicknesses of H, L, and D are all taken to be $d_H = d_L = d_D = 120$ nm. The calculated transmittance of this structure at a fixed temperature of 25 °C is shown in Fig. 3, where the transmittance peaks representing defect modes in the PBG are seen. The number of the defect modes is indeed equal to m, the stack number of PQW [6]. With the appearance of multiple peaks, the structure is used to function as a multichannel narrowband transmission filter which is, in view of spectral efficiency, obviously superior to the usual single-channel multilayer Fabry-Perot resonator [5]. The purpose this paper is to investigate how these defect modes can be shifted by the temperature change, that is, we are interested in the temperature tuning for this multichannel filter.

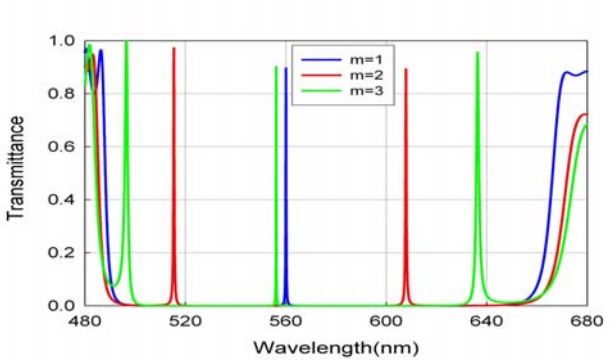

Fig. 3. The defect modes in the PBG of $(HL)^4$ $(BGO/L)^m$ $(HL)^4$.

The temperature dependence includes two factors. The first is that the thicknesses of the constituent layers are a function of the temperature due to the thermal expansion. The second is that the index of refraction of the each layer can be varied as the temperature changes because of the thermal-optical effect. For the thermal expansion, the thickness d of each layer is written as,

$$d(T) = d_0\left(1+\alpha\ \Delta T\right), \tag{7}$$

where α is the thermal expansion coefficient, and ΔT is the temperature deviation. The thermal expansion coefficient α of Si, SiO_2, and BGO are 2.6×10^{-6}/°C, 5.5×10^{-7}/°C, and 6.3×10^{-6}/°C, respectively [21, 22]. For the thermal-optical effect, the temperature dependence of index of refraction n of each layer is

$$n(T) = n_0 + \beta\ \Delta T, \tag{8}$$

where β is the thermo-optic coefficient. The thermal- optic coefficient of Si, SiO_2, and BGO are 1.86×10^{-4}/°C, 1×10^{-5}/°C, and 3.9×10^{-5} /°C, respectively [22, 23].

By incorporating both Eqs. (7) and (8), the calculated transmittance spectra for $(HL)^4(BGO/L)^1(HL)^4$ at four different temperatures, T = 25 (ΔT = 0°C), 125, 225, and 325 °C, are plotted in Fig. 4. There is only one transmittance peak at m = 1. It is seen that the transmittance peak inside the PBG is red-shifted as the temperature increases. The shifting behavior can be explained by using the propagation matrix in Eq. (3) and the phase equation in Eq. (4). When the thickness d and index of refraction n of each layer increase, the wavelength λ must increase accordingly to obtain the same phase change ϕ. The peak wavelengths at various temperatures for $(HL)^4(BGO/L)^1(HL)^4$ are summarized in Table 1. The temperature variation results in the wavelength shift of about 2 nm per 100 °C.

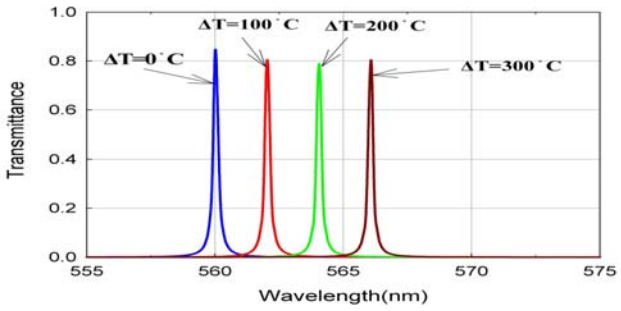

Fig. 4. The transmittance peak of $(HL)^4(BGO/L)^1(HL)^4$ at four different temperatures.

Table 1. The peaks wavelengths at four different temperatures for the structure of $(HL)^4(BGO/L)^1(HL)^4$.

Temperature increment (°C)	Peak wavelength (nm)
0	560.0
100	562.0
200	564.1
300	566.1

Next we present the transmittance spectra for $(HL)^4(BGO/L)^2(HL)^4$ at four different temperatures of 25, 125, 225, and 325 °C. In this case, m = 2, two resonant peaks appear, as illustrated in Fig. 3, where the first peak is near 515 nm and the second is near 610 nm. The effects of temperature on the first and second peaks are plotted in Fig. 5 and 6, respectively. Both are red-shifted as the temperature increases.

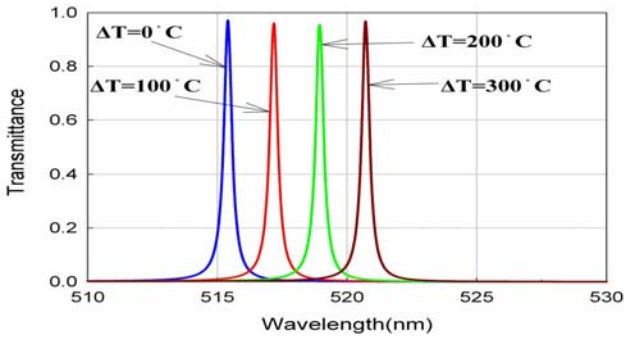

Fig. 5. The first peak of $(HL)^4(BGO/L)^2(HL)^4$ at four different temperatures.

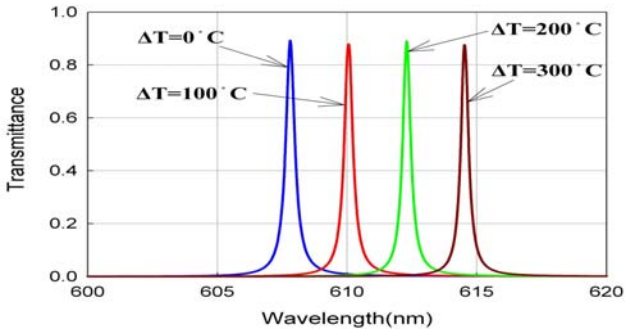

Fig. 6. The second peak of $(HL)^4(BGO/L)^2(HL)^4$ at four different temperatures.

The two peak wavelengths, $\lambda_{p,1}$ and $\lambda_{p,2}$, at four various temperatures for $(HL)^4(BGO/L)^2(HL)^4$ are summarized in Table 2. For each temperature increment of 100 °C, the wavelength shift is about 1.77 nm for the first peak, and 2.23 nm for the second peak.

Table 2. The wavelengths of the transmittance peaks in the PBG for the structure of $(HL)^4(BGO/L)^2(HL)^4$.

Temperature increment (°C)	**$\lambda_{p,1}$ (nm)**	**$\lambda_{p,2}$ (nm)**
0	515.4	607.8
100	517.2	610.1
200	518.9	612.3
300	520.7	614.5

For $m = 3$, we have three resonant peaks, as shown in Fig. 3, where the first peak locates near 500 nm, the second near 560, and the third peak near 640 nm, respectively. We separately plot the temperature dependence for these three peaks in Figs. 7-9.

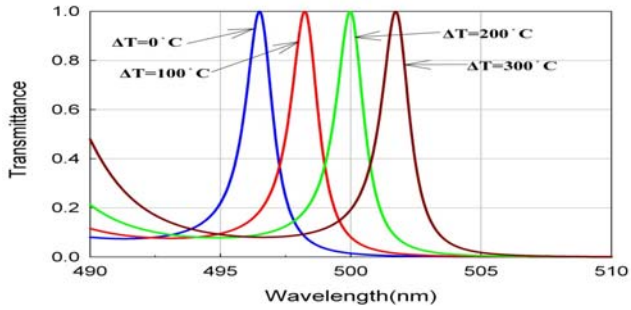

Fig. 7. The first peak of $(HL)^4(BGO/L)^3(HL)^4$ at different temperatures.

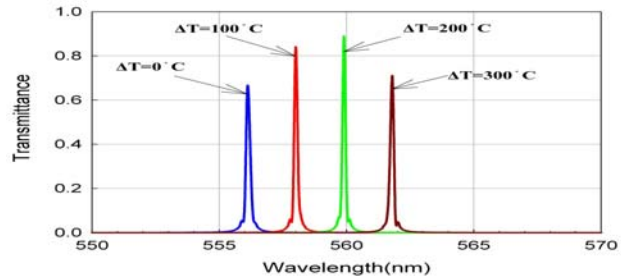

Fig. 8. The second peak of $(HL)^4(BGO/L)^3(HL)^4$ at different temperatures.

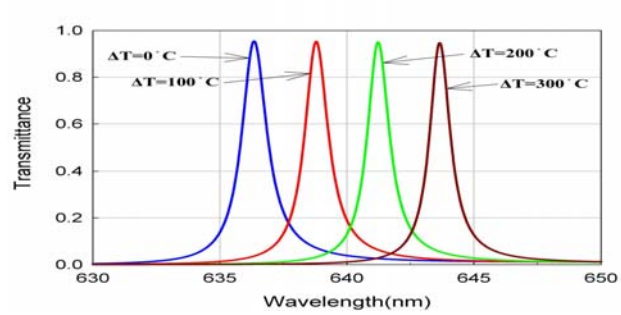

Fig. 9. The third peak of $(HL)^4(BGO/L)^3(HL)^4$ at different temperatures.

The three peak wavelengths, $\lambda_{p,1}$, $\lambda_{p,2}$ and $\lambda_{p,3}$, at four various temperatures for $(HL)^4(BGO/L)^3(HL)^4$ are summarized in Table 3. It can be seen that for each temperature increment of 100 °C, the wavelength shift is about 1.73 nm for the first peak, 1.90 nm for the second peak, and 2.43 nm for the third peak.

Table 3. The wavelengths of the transmittance peaks in the PBG for the structure of $(HL)^4(BGO/L)^3(HL)^4$.

Temperature increment (°C)	$\lambda_{p,1}$ (nm)	$\lambda_{p,2}$ (nm)	$\lambda_{p,3}$ (nm)
0	496.5	556.1	636.3
100	498.2	558.0	638.8
200	500.0	559.9	641.2
300	501.7	561.8	643.6

Table 4. The wavelength shifts per 100 °C of temperature change for the structure of $(HL)^4(BGO/L)^m(HL)^4$, where m = 1, 2, and 3.

Value of *m*	Shift of peak wavelength per 100 °C		
1	2 nm		
2	1.77 nm	2.23 nm	
3	1.73 nm	1.90 nm	2.43 nm

Table 4 summarizes the wavelength shifts of transmittance peaks per 100 °C of temperature change for m = 1-3. According to Table 4 and Figs. 4-9, the third transmittance peak of m = 3 is most sensitive to temperature (2.43 nm per 100 °C), whereas the second transmittance peak of m = 3 is the sharpest.

3.2 Bias voltage dependence of defect modes

We now turn our attention to the voltage dependence of the defect modes. We replace the D layers in the PQW of $(DL)^m$ (shown in Fig. 1(b)) with a nonlinear optical material, namely $LiNbO_3$ (LNO). The index of refraction of LNO is 2.25 at zero bias voltage. The overall structure remains $(HL)^4(DL)^m(HL)^4$, where H and L remain to be Si and SiO_2, respectively. The thickness of H, L, and D layers is 120 nm. Similar to the structure of $(HL)^4(BGO/L)^m(HL)^4$, the number of defects in the PBG of $(HL)^4(LNO/L)^m(HL)^4$ is equal to the number of periods of defect layer m. The results for m = 1 - 3 at 25 °C are shown in Fig. 10. The defect states can be greatly applied in many fields such as diode laser, non-threshold laser, dense wavelength division multiplex, and PC fiber [16], as well as multichannel transmission filter.

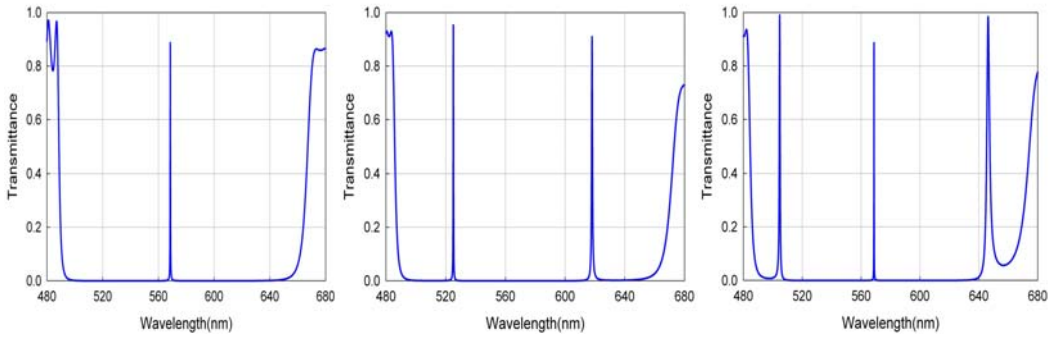

Fig. 10 The defect modes in the PBG of $(HL)^4(LNO/L)^m(HL)^4$, where m = 1 is the left panel, m = 2 is the central panel, and the right panel is for m = 3.

When an external voltage is applied to the LNO layer, as depicted in Fig. 11 taking m = 2 for example, its index of refraction will change with the electric field due to the electro-optic effect. The relation can be expressed as [16]

$$n'_{LNO} = n_{LNO} - \frac{1}{2} n_{LNO}^3 \cdot \gamma_{LNO} \cdot E, \qquad (9)$$

where γ_{LNO} is the electro-optic coefficient of the LNO, with the value of 3.09×10^{-11} m/V, and E is the externally applied electric field. The relation between E and the external applied voltage V is $E = V$ / (0.4 mm), where 0.4 mm is the distance between the electrode pair.

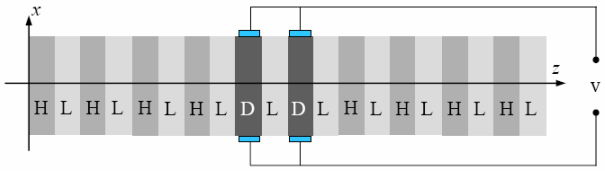

Fig. 11. Schematic biasing-circuit diagram of an $(HL)^4(DL)^2(HL)^4$ 1D PC. The planes of the layers are parallel to the x–y plane. The external voltage is applied along the x-direction, and the light propagates along the z-direction. The thickness of H, L, and D layers is 120 nm.

For m = 1 with a structure of $(HL)^4(LNO/L)^1(HL)^4$, the voltage dependence of the transmittance peak in the PBG is shown in Fig. 12. The wavelengths of peaks are summarized in Table 5. The voltage dependence of transmittance peak is about 0.129 nm for a voltage change of 1 kV.

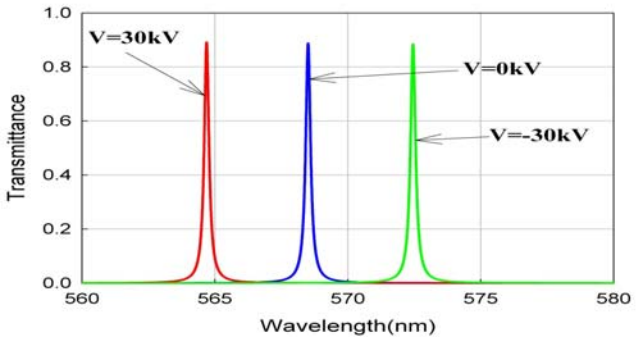

Fig. 12. The transmittance peak in the PBG of $(HL)^4(LNO/L)^1(HL)^4$ at different biases.

Table 5. The wavelengths of peaks for $(HL)^4(LNO/L)^1(HL)^4$.

External applied bias (kV)	Transmittance peaks
30	564.69 nm
0	568.51 nm
–30	572.45 nm

For m = 2, we have the structure of $(HL)^4(LNO/L)^2(HL)^4$. The voltage dependence of the transmittance peaks in the PBG is shown in Fig. 13. The wavelengths of peaks are summarized in Table 6. For the first transmittance peak, the shift is about 0.153 nm for a voltage change of 1 kV. For the second peak, the shift is about 0.149 nm per 1 kV.

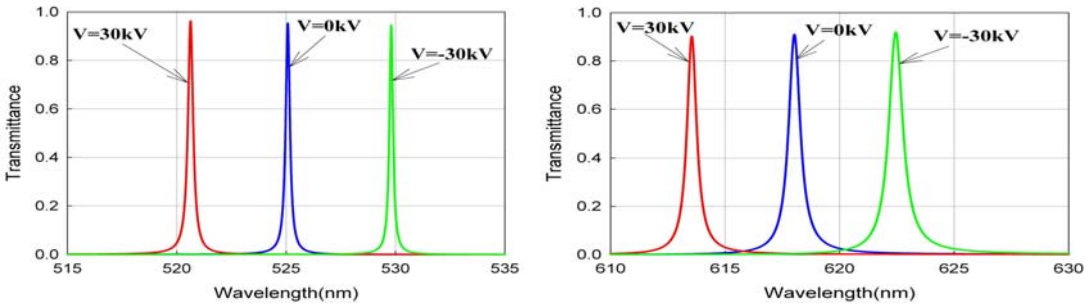

Fig. 130 Voltage dependence of the first peak (left panel), and the second peak (right panel) of $(HL)^4(LNO/L)^2(HL)^4$.

Table 6. The peak wavelengths for $(HL)^4(LNO/L)^2(HL)^4$.

External bias (kV)	$\lambda_{p,1}$	$\lambda_{p,2}$
30	520.63 nm	613.54 nm
0	525.07 nm	618.02 nm
–30	529.80 nm	622.45 nm

Let us continue to examine the case of m = 3, i.e., the structure is $(HL)^4(LNO/L)^3(HL)^4$. The voltage dependence of the transmittance peaks in the PBG are shown in Fig. 14. The peaks wavelengths at different biases are summarized in Table 7. For the first transmittance peak, the shift is about 0.141 nm for a voltage change of 1 kV. For the second peak, the shift is about 0.188 nm per 1 kV. For the third peak, the shift is about 0.137 nm per 1 kV.

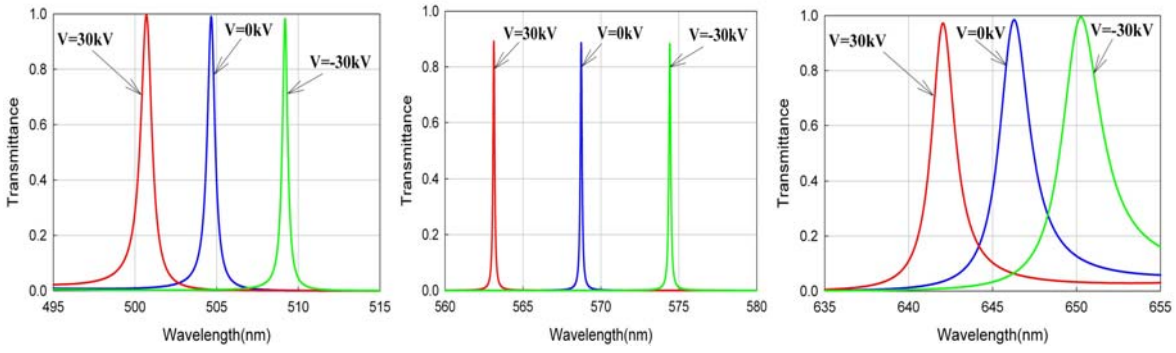

Fig. 140 Voltage dependence of the first peak (left), the second peak (middle), and the third peak (right) of $(HL)^4(LNO/L)^3(HL)^4$.

Table 7. The wavelengths of peaks for $(HL)^4(LNO/L)^3(HL)^4$.

Applied bias (kV)	First peak	Second peak	Third peak
30	500.70 nm	563.13 nm	642.04 nm
0	504.66 nm	568.73 nm	646.28 nm
–30	509.18 nm	574.42 nm	650.26 nm

Table 8 summarizes the wavelength shifts of transmittance peaks in the PBG per 1 kV of applied voltage for m = 1-3. According to Figs. 12~14 and Table 8, the second peak of m = 3 is most sensitive to voltage, and it is also the sharpest peak.

Table 8. The wavelength shifts per 1 kV of applied voltage for the structure of $(HL)^4(LNO/L)^m(HL)^4$, where m = 1, 2, and 3.

Value of m	Shift of peak wavelength per 1 kV		
1	0.129 nm		
2	0.153 nm	0.149 nm	
3	0.141 nm	0.188 nm	0.137 nm

3.3 Complementary comparison

We have so far demonstrated the tunable features for the multichannel filter based on the use of the PQW photonic crystal structure. In scheme 1, the temperature dependence is shown whereas the bias dependence is illustrated in scheme 2. Indeed, there have been many reports that also are related to the PQW structures. In our previous work [24], we have shown that PQW can be used as a defect layer that can cause the transmission and reflection peaks to be tunable in a transmission-and-reflection filter. However, in that special type of filter, the feature of the multichannel cannot be obtained. In the original PQW design [6], the authors first proposed the design for realizing the multichannel filter. In this work, we have shown that how these multiple channels can be tuned by the temperature and the bias as well.

4. Conclusion

Temperature and bias dependences of defect modes in the visible region in the PC containing PQW defect have been investigated. The shift of transmittance peak per 100 °C is in the range of 1.77-2.43 nm. The third transmittance peak of m = 3 is most sensitive to temperature (2.43 nm per 100 °C), whereas the second transmittance peak of m = 3 is the sharpest. The bias dependence is studied by considering the electro-optic effect of the defected layer. The shift of transmittance peaks is in the range of 0.129-0.188 nm for 1 kV of applied voltage. The second transmittance peak of m = 3 is most sensitive to voltage, and it is also the sharpest peak.

In addition to the tunable multichannel filters, the study suggests some potential applications such as the temperature-sensitive sensor, the bias-sensitive sensor, and the refractometric optical sensor. For instance, by selecting temperature- or bias-dependent materials for the constituents in the PQW, a slight movement in the transmission peaks can be observed, which, in turn, can be employed to design a sensor. Moreover, the shifting feature in the transmission peaks is something like a tunable Fabry-Perot interferometer, which can be used as an optical spectrum analyzer.

References

[1] E. Yablonovitch, Phys. Rev. Lett. **58**, 2059 (1987).
[2] S. John, Phys. Rev. Lett. **58**, 2486 (1987).
[3] G. Boedecker, C. Henkel, Opt. Express **11**, 1590 (2003).
[4] Y. Akahane, T. Asano, B. S. Song, S. Noda, Nature **425**, 944 (2003).
[5] S. J. Orfanidis, Electromagnetic Waves and Antennas, Ch. 6, Rutgers University, www.ece.rutgers.edu/~orfanidi/ewa (2008).
[6] F. Qiao, C. Zhang, J. Wan, J. Zi, Appl. Phys. Lett. **77**, 3698 (2000).
[7] X. Chen, W. Lu, S. C. Shen, Solid State Commun. **127**, 541 (2003).
[8] T. Bian, Y. Zhang, Optik **120**, 736 (2009).
[9] C. S. Feng, L.-M. Mei, L. Z. Cai, P. Li, X. L. Yang, Solid State Commun. **135**, 330 (2005).
[10] C. Xu, X. Xu, D. Han, X. Liu, C. P. Liu, C. J. Wu, Optics Commun. **280**, 221 (2007).
[11] S. H. Xu, Z.H. Xiong, L.L. Gu, Y. Liu, X.M. Ding, J. Zi, X.Y. Hou, Solid State Commun. **126**, 125 (2003).
[12] S. Yano, Y. Segawa, J. S. Bae, Phys. Rev. B **63**, 153316 (2001).
[13] H. Němec, L. Duvillaret, F. Garet, P. Kužel, P. Xavier, J. Richard, D. Rauly, J. Appl. Phys. **96**, 4072 (2004).
[14] H. Němec, P. Kužel, L. Duvillaret, A. Pashkin, M. Dressel, M. T. Sebastian, Opt. Lett. **30**, 549 (2005).

[15] L. H. Domash, Optical Interference Coatings (OIC), Optical Society of America, ThB2 (2004).
[16] Q. Zhu, Y. Zhang, Optik **120**, 195 (2009).
[17] S. Eliahou-Niv, R. Dahan, G. Golan, Microelectron. J. **37**, 302 (2006).
[18] T. D. Drysdale, R. J. Blaikie, D. R. S. Cumming, Appl. Phys. Lett. **83**, 5362 (2003).
[19] T. D. Drysdale, I. S. Gregory, C. Baker, E. H. Linfield, W. R. Tribe, D. R. S. Cumming, Appl. Phys. Lett. **85**, 5173 (2004).
[20] P. Yeh, Optical Waves in Layered Media, John Wiley & Sons, Singapore (1991).
[21] S. P. Singh, K. Pal, A. Tarafder, M. Das, K. Annapurna, B. Karmakar, Bull. Mater. Sci. **33**, 33 (2010).
[22] P. A. Williams, A. H. Rose, K. S. Lee, D. C. Conrad, G. W. Day, P. D. Hale, App. Optics **35**, 3562 (1996).
[23] W. N. Ye, R. Sun, J. Michel, L. Eldada, D. Pant, L. C. Kimerling, 5th IEEE International Conference on Group IV Photonics, Sorrento, Italy, 401 (2008).
[24] Y.-H. Chang, C.-C. Liu, C.-J. Wu, Opt. Rev. **17**, 495 (2010).

*Corresponding author: jasperwu@ntnu.edu.tw